RSC Advances

ROYAL SOCIETY OF CHEMISTRY

www.rsc.org/advances

RSC Advances

RSCPublishing

COMMUNICATION

Synthesis and application of ultra-long $Na_{0.44}MnO_2$ submicronslabs as a cathode material for Na-ion batteries†

Cite this: DOI: 10.1039/x0xx00000x

Maowen Xu,†*[ab] Yubin Niu,†[ab] Chuanjun Chen,[ab] Jie Song,[c] Shujuan Bao[ab] and Chang Ming Li*[ab]

Received 00th January 2012,
Accepted 00th January 2012

DOI: 10.1039/x0xx00000x

www.rsc.org/

A novel ultra-long $Na_{0.44}MnO_2$ submicronslabs were fabricated through the sol-gel method followed by high-temperature calcination. The material has a thickness ranging from 100 to 250 nm and a length varying over 10 μm to 40 μm. The electrochemical characterization indicates that the material can deliver a high capacity larger than 120 mAh g^{-1} with stable cycling over 100 in assembled non-aqueous Na-ion cells, the good performance of which mainly attributes to the shortenning sodium ion diffusion distance.

Among various energy storage devices, Li-ion batteries have attracted most research attention mainly due to its high energy density and relatively high power density. [1] However, the high cost of lithium salt and safety issue have been the blockage for the broad applications of the batteries in electric vehicles and grid storage. Based on the abundant availability and low cost of sodium, ambient temperature sodium-based batteries have shown great potential to replace the Li-ion one for green energy storage needs. [2]

There are still great challenges for performance of the Na-ion batteries to catch up with Li-ion technology, and thus it is essential to explore new high capacity sodium-based energy storage materials or to improve the known sodium compounds suitable for Na-ion cells. [3] The sodium manganese oxide such as $NaMnO_2$, $Na_{0.67}MnO_2$, $Na_{0.60}MnO_2$, $Na_{0.44}MnO_2$ and other Na compounds ($Na_xMn_yA_z$, A=transition metal) has been considered as a promising cathode material owing to the high capacity and low cost. [4-9] In general, The sodium manganese oxide mainly has two kinds of structures, layered such as $Na_{0.67}MnO_2$ or tunnelled e.g. $Na_{0.44}MnO_2$ structure, and both have large available numbers of vacancies for the accommodation of Na ions, [10] among which $Na_{0.44}MnO_2$ is particularly attractive because of its unique 3D crystal structure to greatly facilitate Na^+ mobility while stabilizing sodium ions against the conversion into spinel for better cyclability.

$Na_{0.44}MnO_2$ materials can be synthesized via versatile approaches such as solid-state route [11-17], glycine-nitrate combustion [11, 14, 15], hydrothermal synthesis [18, 19], Thermo-chemical conversion [20], polymer-pyrolysis [21] and molten salt synthesis [22]. Sauvage et al. [13] prepared $Na_{0.44}MnO_2$ following the solid state synthesis route, which showed a reversible insertion and extraction of Na ions in $Na_{0.44}MnO_2$ with an initial capacity of 80 mAh g^{-1} at 0.1C rate; however, only half of the initial capacity was retained after 50 cycles, displaying poor cyclability mainly due to failure of the $Na_{0.44}MnO_2$ lattice caused by the large Na ion insertion and extraction. Different approaches including the solid state method followed by mixing with carbon nanotubes (CNTs)[5], polymer-pyrolysis process[17], hydro-thermal approach[18] and chemical route via thermo-chemical conversion to synthesize $Na_{0.44}MnO_2$-CNT composites, nanowires of $Na_{0.44}MnO_2$, showing a nanowires of $Na_{0.44}MnO_2$ with very large surface area and single crystal powders of $Na_{0.44}MnO_2$, respectively for improved capacity cyclability. However, the solid state reaction approach as discussed above has poor dispersion and large particle size to affect the battery performance. Both $Na_{0.44}MnO_2$ and sol-gel method are known but efforts with sol-gel methods are continuously paid to create different unique $Na_{0.44}MnO_2$ materials. [20, 22-24] In this work, we used sol-gel method by using a different processing procedure as well as different chelating agent to well control the material morphology and structures for synthesis of a slab-like $Na_{0.44}MnO_2$ material with good dispersity, ultra-long length and much thinner thickness in the sodium ion deintercalation direction for a high capacity over 120 mAh g^{-1} and stable cycling performance over 100 cycles. It is also revealed that the diffusion distance of sodium ion is

reduced in the obtained material to effectively improve the performance of sodium ion battery.

To synthesize the unique $Na_{0.44}MnO_2$ samples, a stoichiometric amount of $NaNO_3$ (with a 10% excess of sodium), $Mn(NO_3)_2$ (50 wt% aq.) were dissolved in distilled water and stirred for 30 min to form a mixed solution. Then the mixed solution was added dropwise into a 60 wt% critic acid solution. The resulting solution was heated to 90 °C and stirred for 4 h to obtain a clear and viscous gel. The resulting gel was dried at 120 °C for 12 h to produce the precursor. The solid precursor was then ground and heat-treated at 450 °C in air for 6 h to decompose the nitrate and eliminate the water. After cooling down to room temperature, the powdered precursor was ground again, pelletized and then calcined at 900 °C for 15 h in air to obtain the final product.Crystal structure of the obtained samples was characterized by powder X-ray diffraction (XRD, MAXima-X XRD-7000). Furthermore, the morphology and microstructure were examined by field-emission scanning electron microscopy (SEM, JSM-6700F) and transmission electron microscopy (TEM, JEM-2100).For the electrochemical test, the cathode materials were evaluated in 2032 type coin cells using a Na disk as counter electrode and 1 M $NaClO_4$ in ethylene carbonate/diethyl carbonate (EC/DEC, 50 : 50 vol%) solution as electrolyte. The cathode film was prepared by mixing the active material (80 wt %), acetylene black (10 wt%) and polyvinylidene fluoride (PVdF 10 wt %) in N-methyl-pyrrolidinone (NMP) into an electrode slurry and then casting the slurry on aluminium foil collector and dried overnight in vacuum at 120 °C. The assembly of the cells was carried out in a dry Ar-filled glove box. The galvanostatic charge/discharge tests were performed on a LAND cycler (Wuhan Kingnuo Electronic Co., China). Cyclic voltammetric measurements were carried out at a scan rate of 0.25 mV s^{-1} and 0.1 mV s^{-1} using a CHI 660e electrochemical workstation (Chen Hua Instruments Co., China).

$Na_{0.44}MnO_2$ is isostructural to $Na_4Mn_4Ti_5O_{18}$ and crystallizes in an orthorhombic structure (space group: *Pbam*). Fig. 1a schematically shows that the framework of $Na_{0.44}MnO_2$ is built on MnO_5 pyramids and MnO_6 octahedra. These two kinds of polyhedra are interconnected by sharing corners to form two types of unique 1D tunnels. Thus, the prepared $Na_{0.44}MnO_2$ is 3D crystal structure with interconnected unique 1D tunnels as that reported in previous work. [10, 25] Na1 sites are located in the smaller tunnels while Na2 and Na3 are situated in the large S-shaped tunnels. These tunnels serve as diffusion paths for free transport of Na^+ ions mainly along the c-axis direction.The XRD pattern in Fig. 1b shows that the prepared $Na_{0.44}MnO_2$ material crystallizes well in the orthorhombic $Na_4Mn_9O_{18}$ phase (PDF card No: 27-0750).

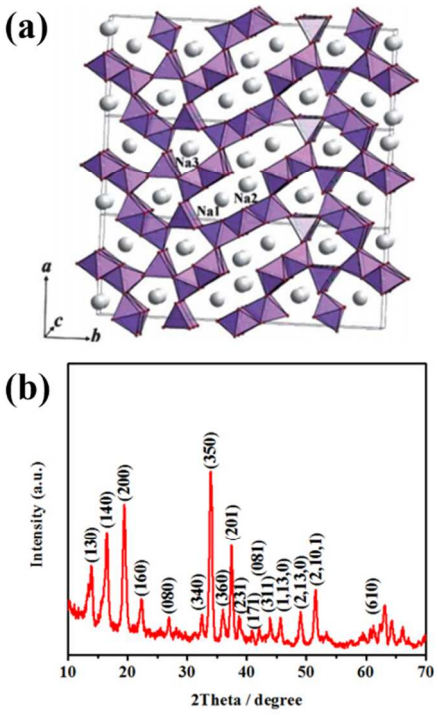

Fig. 1 (a) Crystal structure model of orthorhombic $Na_{0.44}MnO_2$ (adapted from ref. [20]). (b) XRD pattern of as-prepared $Na_{0.44}MnO_2$ materials.

The SEM image shows that pristine $Na_{0.44}MnO_2$ has a slab-like shape with scales of >20 μm (Length)x ~1μm (Width) x ~100 nm to 250 nm (Thickness) (Fig. 2a). The SEM and TEM image in Fig. 2(b) clearly show there is a wide range of width of $Na_{0.44}MnO_2$ varying from submicron to micron.The TEM high resolution image (HRTEM) in Fig. 2c displays a clear lattice fringes corresponding to (200) plane of $Na_{0.44}MnO_2$ while inhiting that the through thickness orientation is along [001], which is consistent with Zhou's report [20]. As discussed above, [001] plane is perpendicular to the c axis allowing sodium ions deintercalation along the thickness direction. Fig. 2d is schematically to represent the morphology and sodium ion deintercalation mechanism. In the synthesis conditions described in the experimental section, sodium manganese oxygen tends to the growth direction of [010], which is along the b axis direction for formation of a flat topography. During the charge-discharge cycles sodium ions intercalation and deintercalation should go through the large S-type channel along the c axis direction. This in turn tells that reduction of the thickness in the c axis direction can shorten the diffusion distance of sodium ion, which is known pronounce parameter to greatly enhance the cycle and rate performance of an ion intercalation-based battery. The diffusion coefficient (D_{Na+}=2.64x$10^{-14}$$cm^2$ s^{-1}) was calculated from our measured impedance data based on the reported method. [10]

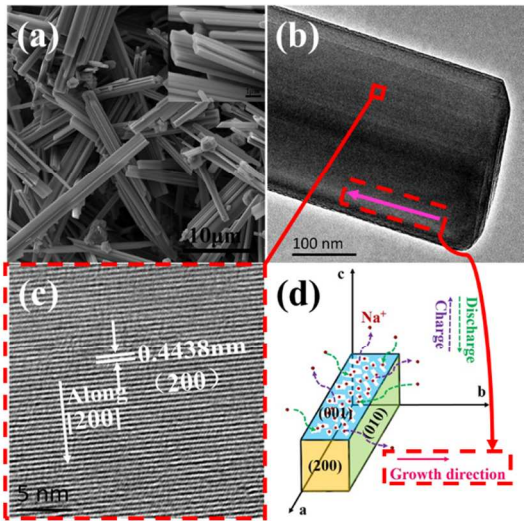

Fig. 2 (a) SEM images (the higher right inset shows high magnification image), (b) TEM image, (c) high-resolution TEM image, (d) morphogenesis and sodium ion deintercalation mechanism of the $Na_{0.44}MnO_2$ submicronslabs.

Fig. 3a shows the galvanostatic charge-discharge capacities at 0.1C rate, indicating excellent cyclability with a capacity retention of 100% even after 100 cycles and a coulombic efficiency of more than 90%. It is worthy of a note that the coulombic efficiency only achieves 90% after the 10th prolonged cycle (Fig. 3a). It is very possibly attributed to the slow electrode activation for the electrolyte to completely penetrate into the inner porous material surface. The different galvanostatic charge-discharge cycles (Fig. 3b), show that the specific capacity of the first charge cycle is higher than the theoretical capacity (121 mAh g^{-1}), whereas the closely followed discharge cycle with one close to the theoretical value. The extremely high capacity in the first charge cycle could be ascribed to extraction of the excess Na ions from Na1 and Na2 sites in the as-prepared material as reported. [20] However, in the consecutive cycles the amount of Na ions detercalated off the electrode should be decreased the thermodynamic limit for a stable crystal structure.

Fig. 3b illustrates that each charge and discharge cycle has multiple-steps, which is in agreement with the reported six biphasic transitions. [13] For further examination of the electrochemical characteristics and cyclability of the prepared sample we conducted cyclic voltammetry (C-V) studies before and after cycles. The CV curves in Fig. 3c also indicate reversibility of the six biphasic transitions during the anodic and cathodic sweeps as observed from the galvanostatic charge-discharge cycles with steps and show very consistent reversibility of Na insertion and extraction before and after cycles. The distance between the discharge and charge curves is small, indicating a low electrochemical polarization. [26] As seeing in Fig. 3d, the difference $\Delta E_{after\ cycles}$ between oxidation and reduction peaks increases after the cycles. It is caused mainly by the more positive oxidation peak than that before cycling, indicating a deintercalation polarization developing with the increased number of cycles while the intercalation process does not have significant polarization.

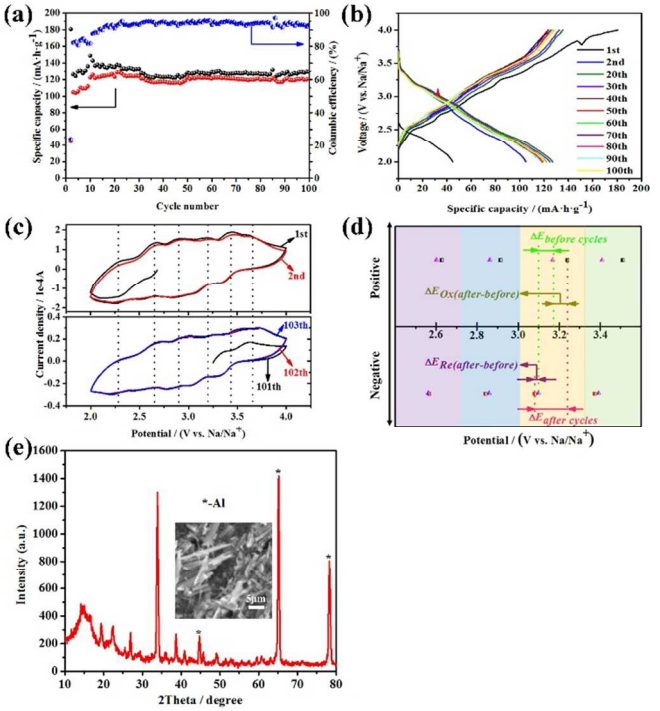

Fig. 3 (a) Galvanostatic charge-discharge cyclability and coulombic efficienecy, (b) different galvanostatic charge-discharge cycles, (c) cyclic voltammorgm plots before and after cycles of the cathode samples against the Na electrode at a scan rate of 0.1mV/s, (d) schematic illustration for the oxidation-reduction peaks shift before and after cycles, and (e) XRD pattern and SEM image (inset) of as-prepared $Na_{0.44}MnO_2$ materials after 100 cycles at 0.1C.

A rationally fabricated structure of the electrodes is able to play an essential role in improvement of electrode kinetics for better performance of an ion intercalation-based battery, which requires a nanostructure to have not only more activation sites for reversible ion inter-/detercalation process but also enhanced mass transport by reduced diffusion distances for Na ion intercalation during the charge-discharge cycles. Although the length and width of the slab of the $Na_{0.44}MnO_2$ crystals are in the submicron to micron range, their thickness direction along [001] , c-axis could facilitate easy intercalation of Na ions to achieve the theoretical capacities while accommodating the strains with Na ion insertion into the material. Fig. 3e shows that XRD pattern scarcely has any change besides the intensity of peaks, thus evidencing that the submicronslabs can retain its intact crystal structure for long charge/discharge cycles.

In summary, a ultra-long $Na_{0.44}MnO_2$ submicronslabs were fabricated through the sol-gel method followed by high-temperature calcination. Results show that the $Na_{0.44}MnO_2$ submicronslabs-based Na ion battery achieves its theoretical capacity value over 100 cycles, which attribute mainly to decreased sodium ion diffusion distance and the stable crystal structure.

This work is financially supported by Chongqing Key Laboratory for Advanced Materials and Technologies of Clean

Energies under cstc2011pt-sy90001, Start-up grant under SWU111071 from Southwest University and Chongqing Science and Technology Commission under cstc2012gjhz90002. The work is also supported by grants from the National Natural Science Foundation of China (no. 21063014, 21163021 and 51101130), Fundamental Research Funds for the Cental Universities (SWU113079, XDJK2014C051).

Notes and references

** Corresponding author*
† These authors contributed equally to this work.
[a]Institute for Clean Energy & Advanced Materials, Faculty of Materials and Energy， Southwest University, Chongqing 400715, P.R. China
[b]Chongqing Key Laboratory for Advanced Materials and Technologies of Clean Energies, Chongqing 400715, P.R. China
[c],Texas Materials Institute, University of Texas at Austin, Texas 78712, USA
Fax: +86-23-68254969; Tel:+86-23-68254969; E-mail: xumaowen@swu.edu.cn and ecmli@swu.edu.cn

1. R. Marom, S. F. Amalraj, N. Leifer, D. Jacob and D. Aurbach, *J. Mater. Chem.*, 2011, 21, 9938-9954.
2. X. Liu, N. Zhang, J. Ni and L. Gao, *J. Solid State Electr.*, 2013, 17, 1939-1944.
3. B. L. Ellis and L. F. Nazar, *Curr. Opin. Solid St. M.*, 2012, 16, 168-177.
4. J. P. Parant, Olazcuag.R, Devalett.M, Fouassie.C and Hagenmul.P, *J. Solid State Chem.*, 1971, 3, 1-11.
5. D. Yuan, W. He, F. Pei, F. Wu, Y. Wu, J. Qian, Y. Cao, X. Ai and H. Yang, *J. Mater. Chem. A*, 2013, 1, 3895-3899.
6. J. Xu, D. H. Lee, R. J. Clément, X. Yu, M. Leskes, A. J. Pell, G. Pintacuda, X.-Q. Yang, C. P. Grey and Y. S. Meng, *Chem. Mater.*, 2014, 26, 1260-1269.
7. H. Yoshida, N. Yabuuchi, K. Kubota, I. Ikeuchi, A. Garsuch, M. Schulz-Dobrick and S. Komaba, *Chem. Commun.*, 2014, DOI: 10.1039/C3CC49856E.
8. D. Yuan, X. Hu, J. Qian, F. Pei, F. Wu, R. Mao, X. Ai, H. Yang and Y. Cao, *Electrochim. Acta*, 2014, 116, 300-305.
9. H. Zhu, K. T. Lee, G. T. Hitz, X. Han, Y. Li, J. Wan, S. Lacey, A. v. W. Cresce, K. Xu, E. Wachsman and L. Hu, *ACS Appl. Mater. Inter.*, 2014, 6, 4242-4247.
10. L. Zhao, J. Ni, H. Wang and L. Gao, *RSC Adv.*, 2013, 3, 6650-6655.
11. M. M. Doeffa, T. J. Richardsonb, J. Hollingswortha, C.-W. Yuan and M. Gonzales, *J. Power Sources*, 2002, 112, 294-297.
12. F. Sauvage, E. Baudrin and J.-M. Tarascon, *Sensor Actuat B-Chem*, 2007, 120, 638-644.
13. F. Sauvage, L. Laffont, J. M. Tarascon and E. Baudrin, *Inorg. Chem.*, 2007, 46, 3289-3294.
14. J. A. Saint, M. M. Doeff and J. Wilcox, *Chem. Mater.*, 2008, 20, 3404-3411.
15. F. Funabiki, H. Hayakawa, N. Kijima and J. Akimoto, *Electrochem. Solid St.*, 2009, 12, F35-F38.
16. A. D. Tevar and J. F. Whitacre, *J. Electrochem. Soc.*, 2010, 157, A870-A875.
17. J. F. Whitacre, A. Tevar and S. Sharma, *Electrochem. Commun.*, 2010, 12, 463-466.
18. E. Hosono, H. Matsuda, I. Honma, S. Fujihara, M. Ichihara and H. Zhou, *J. Power Sources*, 2008, 182, 349-352.
19. Y. Li and Y. Wu, *Nano Res*, 2009, 2, 54-60.
20. X. Zhou, R. K, Guduru and P. Mohanty, *J. Mater. Chem. A*, 2013, 1, 2757-2761.
21. Y. Cao, L. Xiao, W. Wang, D. Choi, Z. Nie, J. Yu, L. V. Saraf, Z. Yang and J. Liu, *Adv. Mater.*, 2011, 23, 3155-3160.
22. L. GAO, J. NI, H. WANG and L. ZHAO, *Funct. Mater. Lett.*, 2013, 06, 1350012.
23. E. Hosono, T. Saito, J. Hoshino, M. Okubo, Y. Saito, D. Nishio-Hamane, T. Kudo and H. Zhou, *J. Power Sources*, 2012, 217, 43-46.
24. L. Chen, Q. Gu, X. Zhou, S. Lee, Y. Xia and Z. Liu, *Sci. Rep.*, 2013, 3.
25. Q. Feng, H. Kanoh and K. Ooi, *J. Mater. Chem.*, 1999, 9, 319-333.
26. L. Qiu, Z. Shao, M. Liu, J. Wang, P. Li and M. Zhao, *Carbohyd. Polym.*, 2014, 102, 986-992.

